Experimental and Numerical Analysis of Pre-Chamber Combustion Systems for Lean Burn Gas Engines

Author(s):
Shapiro, Evgeniy; Tiney, Nick; Kyrtatos, Panagiotis; Kotzagianni, Maria; Bolla, Michele; Boulouchos, Konstantinos; Tallu, Gunesh; Lucas, Gwendal; Weissner, Michael

Publication date:
2019-04

Permanent link:
https://doi.org/10.3929/ethz-b-000339039

Originally published in:
SAE Technical Papers, https://doi.org/10.4271/2019-01-0260

Funding acknowledgement:
652816 - Gas-Only internal combustion engines (SBFI)

2019-01-0260

Experimental and numerical analysis of pre-chamber combustion systems for lean burn gas engines

Evgeniy Shapiro and Nick Tiney **Ricardo UK Ltd**

Panagiotis Kyrtatos, Maria Kotzagianni, Michele Bolla, and Konstantinos Boulouchos **Swiss Federal Institute of Technology**

Gunesh Tallu, Gwendal Lucas, and Michael Weissner **Volkswagen AG**

Abstract

The current trend in automobiles is towards electrical vehicles, but for the most part these vehicles still require an internal combustion engine to provide additional range and flexibility. These engines are under stringent emissions regulations, in particular, for the reduction of CO2. Gas engines which run lean burn combustion systems provide a viable route to these emission reductions, however designing these engines to provide sustainable and controlled combustion under lean conditions at λ=2.0 is challenging. To address this challenge, it is possible to use a scavenged Pre-Chamber Ignition (PCI) system which can deliver favorable conditions for ignition close to the spark plug. The lean charge in the main combustion chamber is then ignited by flame jets emanating from the pre-chamber nozzles. Accurate prediction of flame kernel development and propagation is essential for the analysis of PCI systems. A modelling approach is proposed based on the Dynamic Discrete Particle Ignition Kernel model coupled with the G-equation combustion model. The model is validated for an air/methane academic benchmark. The approach is then applied to the investigation of performance of three pre-chamber designs developed within Horizon 2020 GASON project in conjunction with the experimental investigation of these pre-chambers mounted on Rapid Compression Expansion Machine (RCEM). The investigated pre-chamber designs vary with respect to the tangential nozzle angle and volume. The study focusses on a lean limit of the proposed system's operation with the main charge at λ=2.0 and a variation of pre-chamber design and scavenging level. The comparison of the simulation results with the experimental observations demonstrates good accuracy of the developed model. In addition, the combined experimental and modelling provides insights into the effect of pre-chamber geometry on potential performance.

Introduction

Pre-chamber Ignition (PCI) systems development for in-cylinder applications has been a subject of a substantial body of research, starting from the pioneering work of Sir Harry Ricardo [1]. More recent trends in the applications of PCI systems are related to the extension of stable operation of the target engine towards lean combustion, with the reduction of emissions being the main objective. Toulson et al. [2] highlight the benefits of lean burn combustion for NOx reduction which can be delivered by a pre-chamber for gasoline engines. Natural gas PCI systems have been extensively explored for heavy-duty and power generation applications. On the other end of the spectrum, PCI systems are used to improve thermal efficiency and increase compression ratio for high performance gasoline engines in Formula 1.

The ignition physics of a PCI system largely depend on the quenching effect within the pre-chamber nozzles. Larger nozzles allow the conventional flame torch operation mode, where the flame front can propagate through the nozzles to the main combustion chamber without or with only partial quenching. Whereas the LAG [3] concept, employed in Turbulent Jet Ignition system (e.g. [4]) relies on smaller nozzle diameters to enable flame quenching in the nozzles, delivering multiple-site ignition from quenched partial reaction products.

The application of pre-chamber ignition systems to extend the lean limit of operation in natural gas engines for the passenger car market at diesel-like compression ratios has received comparatively little attention. The development of such systems is one of the objectives of the Horizon 2020 GASON project [5], prompting the investigation presented in this paper. The pre-chambers considered within the project mainly employ the flame torch mechanism.

The target engine platform is a 1968cm3 displacement engine operating at 14.5 compression ratio described in [6]. The design of the combustion system for the GASON engine has started with the initial idea of downscaling pre-chambers known from large bore engines within the Volkswagen Group to a passenger car size engine, these initial geometries were further modified to improve mixture homogeneity and local stoichiometry in the vicinity of the spark at target spark time [7]. Two of the pre-chambers presented in the current study have been also investigated numerically in conjunction with piston shape optimization in [7].

The design of the PCI systems incorporates a number of variables. A recent summary of the design process for PCI systems for large engines can be found in [8], where the design vectors in relation to pre-chamber volume, nozzle configuration and nozzle angle are examined for large bore engines. The relative volume determines the energy content which can be delivered by the ignition system, while the angle of the nozzles defines the flow topology in the pre-chamber and, consequently - the mixing and combustion process.

In the present work three variants of GASON pre-chambers are investigated with the variation of the volume and nozzle incline. These configurations are investigated in an RCEM experiment and through numerical simulations. In order to relate the experimental and numerical investigation for RCEM-mounted pre-chamber to potential performance in engine conditions, two criteria are proposed. Firstly, the homogeneity level of the mixture in the pre-chamber is evaluated through average and standard deviation of the inverse equivalence ratio in the spark volume. Secondly, the jet nozzle exit time measured from the spark time to the point when the flame

emerges from the pre-chamber nozzles is considered – a more rapid flame propagation through the pre-chamber pointing to a higher flame jet momentum and a better performance of the ignition system.

Experimental Methodology

The current study was performed in a Rapid Compression Expansion Machine (RCEM). The RCEM operates in a single cycle mode (compression-expansion) and combines excellent optical access with high flexibility in independently changing parameters, such as mixture composition, start of ignition, initial chamber conditions, etc. The RCEM uses a free-floating piston which is driven by apneumatic-hydraulic system towards the cylinder head. This motion creates the compression stroke, while the increasing pressure due to compression and combustion eventually drive the piston back. The piston contains a quartz window which allows optical access towards the cylinder head, where the different pre-chambers are mounted centrally. A UV-enhanced mirror is placed behind the quartz piston in order to allow the detection of the area where the reacting jets were exiting and the combustion inside the main chamber. A schematic of the RCEM, showing the most important components, is shown in Figure 1. The most important technical characteristics are summarized in Table 1, while further details about the driving part and the principle of operation of the RCEM can be found in [9].

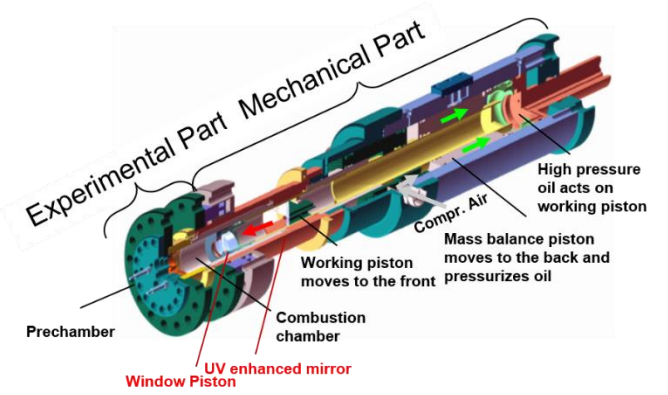

Figure 1. Drawing of the RCEM, adapted from [10]

The RCEM bore diameter is B = 84 mm and the quartz piston has a top hat bowl shape with diameter of 52 mm and depth of 2.2 mm. The piston stroke is adjustable (s=120-250mm), and for this study was set at maximum. The temperature of the cylinder head and liner was set to 383K using different heating elements and measured by 6 K-type thermocouples. Differently than in an engine, the filling process of the RCEM cylinder is occurring well before the compression and thus no turbulence exists in the main chamber at the beginning of the stroke.

The pre-chambers used were all positioned centrally in a plane normal to the cylinder axis, similarly to their placement in an engine cylinder. More details about their geometry can be found in a following section. The pressure measurements inside the pre-chamber and main chamber were performed using a miniature Kistler pressure sensor (M3.5x0.35, 0-250bar), and a cooled piezoelectric pressure sensor (Kistler no. 7061B, 0-250bar), which was coupled to a Kistler 5011 charge amplifier.

Table 1. Technical characteristics of the Rapid Compression Expansion Machine (RCEM)

Parameter	Description
Bore (B)	84 mm
Stroke length (s)	Adjustable from 120-249mm (here 249mm)
Compression stroke (ε)	5-30
Loading pressure (P_{load})	1-3 bar (here 1.2bar)
Max. cylinder pressure (P_{max})	Up to 200 bar
Piston bowl	d_b = 52mm, 2.2mm depth (top hat)
Piston optical access	d_w = 52mm, quartz window
Heating system	Cylinder head and cylinder liner heating
Ignition	Spark plug mounted inside the pre-chamber

An absolute piezoresistive pressure sensor (Kistler no. 4053, 0.0-5.0 bar) was employed for the pressure correction (pegging) of the piezoelectric pressure sensors mounted on the pre-chamber and the main chamber. The pressure sensor was connected to the cylinder through an automatic switching adaptor (Kistler 741A), which allowed the piezoelectric sensor pegging during the early stages of compression. The initial pressure inside the combustion chamber was set at 1.2 bar for all operating points. Additional piezo-resistive pressure sensors were mounted on the driving piston and the fuel supply line of the PC and MC to control the filling of the driving gas, which was set at 27bar, and the fuel pressure for the PC and the MC, which were set to 10 bar and at 60 bar respectively. The synchronisation of all triggering signals, i.e. for the start of injection in the pre- and main chamber, the ignition timing and the image acquisition by high speed camera, was achieved using a pressure and a position based system at certain cylinder pressures and piston positions.

The fuel for the filling of the main chamber was administered by a Siemens hollow cone piezo actuated injector, which was located 35 mm off-axis in the cylinder head. The piezo injector has an umbrella angle of 90 degrees and was operated with a nominal needle lift of 25µm. The injection pressure was 60bar. For safety reasons and in order to achieve a homogeneous background methane-air mixture, the gaseous methane was injected into the chamber filled with pure air (P_{load}=1.2bar) about 3 seconds bTDC and prior to the start of compression. The composition of the main chamber was λ=2.0. The methane injection for filling the pre-chamber was performed using a prototype injector. The injector was supplied with fuel through the standard pre-chamber injector rail, and the rail pressure was kept constant at 10 bar throughout the experiments. The start of injection was performed during the compression, when the pressure of the main chamber reached 2.0 bar. The injection duration for the pre-chamber fuel filling varied from 4.0-10.0ms. The fuel for the PC and MC was supplied from high purity methane bottles (99.995% CH_4). The ignition was initiated by an ignition coil (VW AG 06.J.905.110.G, BEO S3) with a G-type spark plug (NGK R -M10) which has a 0.5mm gap. The pressure at start of ignition was kept constant at 26bar for all measurements performed.

Information about the combustion characteristics of the flame/radical jets and the flame propagation inside the main chamber were acquired using high speed 2D OH* chemiluminescence imaging. The spatial distribution of OH* chemiluminescence was recorded with an

intensified high speed camera at 32 kHz repetition rate (LaVision HSSX and image intensifier, 10/12 bits dynamic range) equipped with a 50 mm UV lens (f/20) and a bandpass filter for a wavelength of 306 nm and 12.1 nm FWHM. The acquired 2D OH* chemiluminescence images have been analysed using a purpose-built Matlab routine in order to obtain information about the jet exiting time.

The challenge of designing the pre-chamber system was to find very compact solutions to package all features within the small available space of the cylinder head of the base engine. The space is smaller than in comparable petrol engines due to the vertically oriented valves, which lead to a narrow positioning of the camshafts. Figure 2 shows the section view of the relevant area illustrating the difficulties to integrate the chamber, gas-feed, check valve, pressure sensor and the spark plug within the narrow tubular area former used by the Diesel high pressure injector. The design is modular and made for an easy access to the components to enable the change of e.g. the chamber without dismantling the engine completely. The bottom part of the system, shown in dark green in Figure 2, is the main component, the pre-chamber, which has been created in different designs to create different shapes, volumes and nozzles. The volume is an interesting parameter to learn about the influence of the involved mass of air and NG in the pre-chamber to the character of the combustion of the lean mix in the main combustion chamber. The design of the nozzle allows for influencing the charge motion in both, the pre-chamber during compression stroke and also in the main combustion chamber during combustion stroke. Those two main parameters have been addressed by the presented comparison of the three shown pre-chambers.

Out of the series of pre-chambers investigated in the GASON project, three shapes were selected to evaluate the nozzle angle and volume effects. The nomenclature and varied pre-chamber parameters are summarized in Table 2. The parameters of the target GASON engine, defined the spatial constraints and available volume with all pre-chambers with the outer diameter of the top section of pre-chamber equal to 13.7mm. All pre-chambers feature 7 nozzles of 1.5mm diameter. The nozzle angle to z-axis is equal to 64.5deg for all cases. Effective volume of the pre-chamber was evaluated by considering the volume above the nozzles only. The shapes of the pre-chambers are illustrated in Figure 3. The spark is oriented with the spark plug gap pointing away from the pre-chamber wall to allow for unconstrained motion of the flame kernel. The figures in the right column of Figure 3 exclude the spark body in order to provide a clear view of the nozzle configuration.

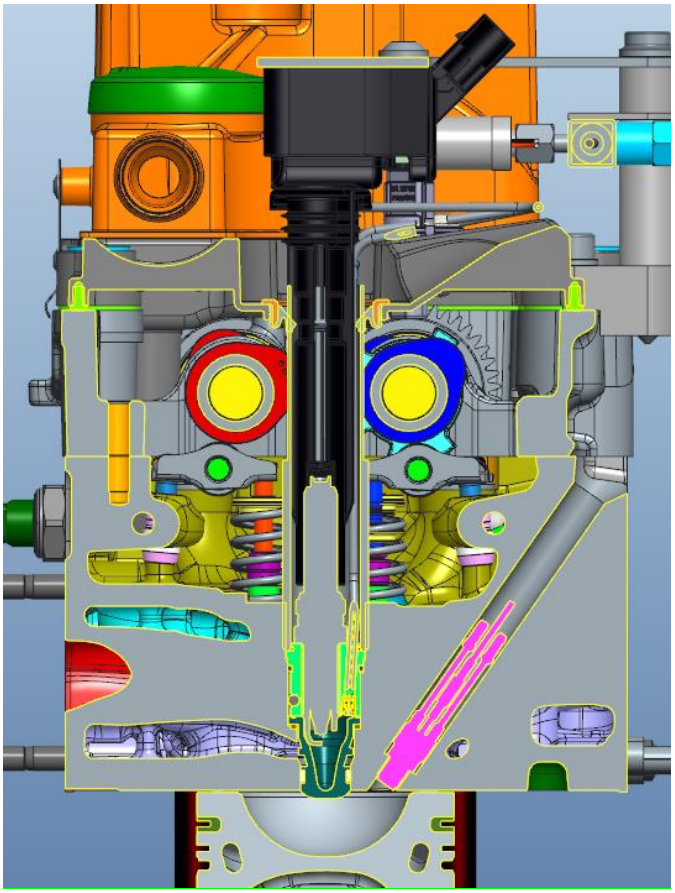

Figure 2. Section view through cylinder head of GASON-engine [11]

Table 2. Pre-chamber parameters

Designation	PC-A (IC1 [7])	PC-C1 (IC2 [7])	PC-D2
Effective volume (m3)	1.7e-06	1.7e-06	2.13e-06
Nozzle tangential position	Inclined	Straight	Straight

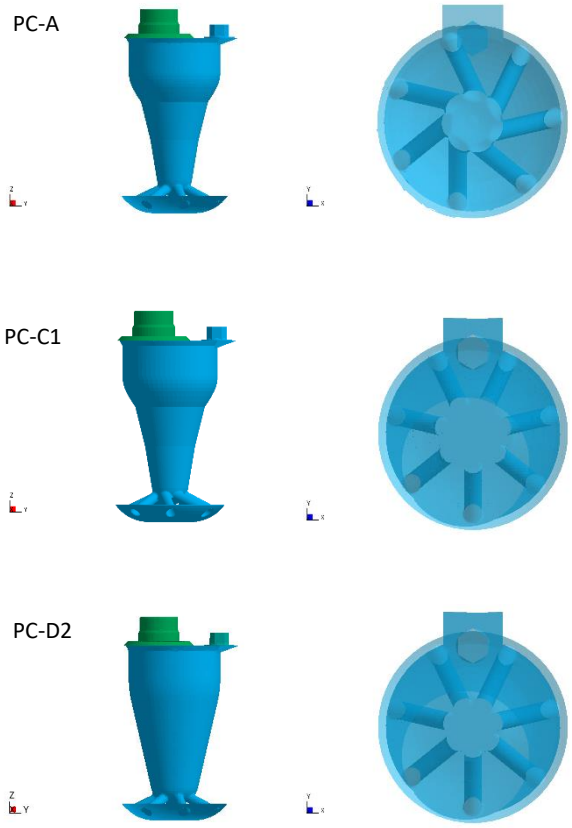

Figure 3. Pre-chamber designs (PC-A, PC-C1, PC-D2)

Experiments were conducted in a series of repetitions, for each nominal injected mass. In each series a representative one was selected for the CFD analysis. Nomenclature of the cases and parameters of the representative realisation are summarised in Table 3, where the timings are based on equivalent rpm of 600 computed from the average RCEM cycle time.

Table 3. Cases nomenclature and essential parameters

	Case	Mass	Injection Start	Injection Duration	Spark Timing
		mg	deg	deg	deg
PC-A	ID001	0.6	645.7	12.6	708.1
	ID002	0.9	645.7	18.0	708.8
	ID003	1.2	646.5	23.4	708.8
	ID004	1.5	647.1	28.8	708.7
	ID005	1.7	647.3	34.2	708.7
PC-C1	ID001	0.6	647.2	12.6	708.1
	ID002	0.9	647.9	18.0	708.7
	ID003	1.2	647.9	23.4	709.4
	ID004	1.5	648.6	28.8	709.3
	ID005	1.7	649.5	34.2	709.5
PC-D2	ID001	0.6	647.0	12.6	708.3
	ID002	0.9	648.1	18.0	709.3
	ID003	1.2	649.7	23.4	710.0
	ID004	1.5	649.4	28.8	710.3
	ID005	1.7	649.4	34.2	710.2

Figure 4 illustrates the standard deviation of the measured jet exit times as a function of the injected fuel mass, providing a quantification of the repeatability of the experiment. The standard deviation is based on six repetitions of the experiment.

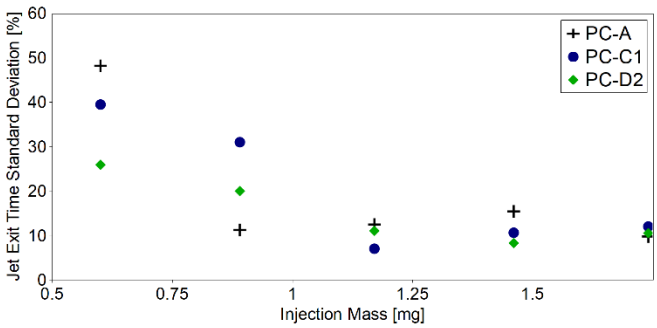

Figure 4. Standard deviation of measured jet exit times

Modelling Methodology

From the CFD perspective, the modelling of flow and combustion in the constrained space of PCI systems poses several distinct challenges. Considering the stages of the simulation, firstly, the interaction between the flow driven by jets formed by pre-chamber nozzles in the compression stage and its interaction with the fuel supply needs to be captured accurately in order to resolve the mixture formation process. Secondly, the development of the initial flame kernel in a highly non-homogenous mixture near the spark plug gap and its motion during the period of spark activity to be captured. Finally, the propagation of flame in the constrained space of the pre-chamber and its interaction with the pre-chamber nozzles needs to be modelled accurately.

Ricardo VECTIS CFD software is used in simulation with a number of dedicated models developed to facilitate PCI systems modelling. The CFD model incorporates recently developed Dynamic Discrete Particle Ignition Kernel (DDPIK) (e.g. [12]) spark model coupled with the G-equation combustion model and Ricardo Two-zone Flamelet Model using 0D chemistry (e.g. [13]). The spark model was developed specifically for the selected application and has been modified for the present study, therefore its formulation is described in more detail. The model extends the methods proposed in [14, 15] and represents the flame kernel development in arc and glow discharge stages as a 1D system which incorporates several sub-models. Firstly, the initial radius r is predicted from the spark parameters using an extension of Sher's two-stage breakdown model [16]:

$$r = \sqrt{\frac{\gamma - 1}{\gamma} \frac{E_{bd}}{P\pi l \left(1 - \frac{T + \frac{LHV}{c_p}}{\left(\frac{1}{\gamma}(T_{bd} - T) + T\right)}\right)}} \quad (1)$$

Where γ is the adiabatic index, E_{bd} and T_{bd} represent the spark breakdown energy and temperature respectively, c_p is the specific heat of the air/fuel mixture, LHV is the lower heating value of the mixture, l is the spark plug gap and P and T refer to pressure and temperature of the ambient gas respectively. The geometry of the NGK M10 tested in the experiment is used in simulations. The breakdown temperature T_{bd} exhibits little variation and a value of 60,000K is appropriate for most cases [17], the break-down energy of 0.1mJ was used based on the validation reported in [12].

Following the initial kernel generation, the evolution of the kernel is described by a 1D system derived from mass and energy conservation

laws and expressed in terms of kernel radius r_k and temperature T_k as follows:

$$\begin{cases} \frac{dr_k}{dt} = Q_{r,f} + Q_{r,e} + Q_{r,c} \\ \frac{dT_k}{dt} = Q_{T,W} + S_{T,f} + Q_{T,c} \end{cases} \quad (2)$$

where subscript "k" is used to denote the kernel radius and temperature. The mass source from flame propagation expressed in terms of temperature under pressure equilibrium conditions is given by:

$$Q_{r,f} = \frac{R_k T_k}{R_u T_u} B \quad (3)$$

where R is the gas constant and the subscript "u" refers to the unburnt side of the flame front. All quantities corresponding to the unburnt side of the flame front are obtained by averaging of the 3D CFD solution sampled at the location of DPIK particles over the set of the particles.

The aggregate burn rate B incorporates modified turbulent flame speed S_T^* and plasma expansion speed as follows:

$$B = S_T^* + \frac{W}{4\pi r_k^2 \rho_u (c_{p,k} T_k - c_{p,u} T_u)} (4)$$

where W stands for the effective (time-averaged) spark power and ρ denotes density. The actual spark power varies quite substantially through the arc and glow phases of the discharge (see, for example, [15]). In the absence of a direct measurement W can be regarded as a tuning parameter. The value of 210W was used based on a study of a similar spark in [12]. The sensitivity of the model to uncertain parameters has been investigated in [18]**.** The modified turbulent flame speed S_T^* taking into account the flame front curvature and laminar and turbulent diffusivity was adopted following [21]:

$$S_T^* = S_T - \frac{2}{r_k}\left(\frac{\nu}{Pr} + 0.28 l_{ft} u'\right) (5)$$

where Pr and ν are laminar Prandtl number and dynamic viscosity respectively. Note that analysis of the laminar counterpart of the above expression points to it corresponding to Markstein number ~1. u' is the turbulent velocity expressed, in the context of homogenous RANS turbulence modelling, through the turbulent kinetic energy k as $u' = \sqrt{\frac{2}{3}k}$. The flame brush thickness of the spark flame front l_{ft} is approximated as follows (e.g. [19,29]):

$$l_{ft} = \sqrt{2 u' l_I t \left(1 - \frac{l_I}{u' t}\left(1 - \exp\left(-\frac{u' t}{l_I}\right)\right)\right)} (6)$$

Where t is the time since ignition t and turbulent integral lengthscale is approximated as $l_I = u'^3/\epsilon$, where ϵ is the turbulence dissipation rate averaged over the flame front.

S_T is the baseline turbulent flame speed. In RANS/CFD modelling context, the formulation of the local turbulent flame speed is far from certain even in the fully turbulent flow regimes. A good extensive discussion of this subject is provided in [29]. Capturing the early stages of the flame kernel evolution requires a transitional formulation of the flame speed. The formulation employed in the present study was proposed in [15], where it was shown to produce accurate results in the context of a more complex kernel model:

$$\frac{S_T}{S_L} = 1 + \left(\frac{u'}{u' + S_L}\left(1 - exp\left(-\frac{r_k}{l_I}\right)\right)\left(1 - exp\left(-\frac{(u' + S_L)t}{l_I}\right)\right)\right)^{\frac{1}{2}} \left(\frac{u'}{S_L}\right)^{\frac{5}{6}} (7)$$

Where laminar speed S_L is given by a correlation for methane modified to extend applicability to lean operation [13,20]. Note that curvature effects are separately incorporated in the flame speed reduction term in Equation (6). The above approach extends the one reported in [12], where a simpler turbulent flame speed correlation was used without transitional effects.

The source term representing the effect of expansion cooling on the kernel radius and external compression source term modelling the effect of piston motion in the mass conservation equation are given by:

$$Q_{r,e} = \frac{r_k}{3}\frac{1}{R_k T_k}\frac{d(R_k T_k)}{dt} (8)$$

and

$$Q_{r,c} = -\frac{r_k}{3}\frac{1}{P_u}\frac{dP_u}{dt} (9)$$

respectively.

Energy conservation source term $Q_{T,W}$ reflects power supply from the ignition coil:

$$Q_{T,W} = \frac{W}{\frac{4}{3}\pi r_k^3 \rho_u}\frac{\gamma_k - 1}{\gamma_k}\frac{T_k}{R_u T_u} (10)$$

The second source term corresponds to the energy spent on the increase of temperature of the acquired fresh mass to that of the kernel and chemical energy released in the associated combustion process.

$$Q_{T,e} = \frac{3}{c_{p,k} r_k}\frac{R_k T_k}{R_u T_u}\left(LHV_{mix} - \left(c_{p,k} T_k - c_{p,u} T_u\right)\right) S_b (11)$$

Finally, similarly to the mass conservation the effects of the change in the ambient unburnt side pressure P_u accounted for:

$$Q_{T,c} = \frac{\gamma_k - 1}{\gamma_k}\frac{T_k}{P_u}\frac{dP_u}{dt} (12)$$

The 1D system is solved numerically with the first order explicit solver and the solution is used to evaluate the position of the flame surface which is discretized into a set of particles covering the sphere of the flame with a uniform random distribution. Simulations for all cases reported in this paper use 20000 particles to discretize the kernel. The required averaged unburnt side values from the 3D

simulation are averaged over the flame front based on the position of the particles. The motion of the kernel is resolved based on the motion of the velocity of the kernel centroid in the 3D simulation. The reaction rate is computed based on the volume swept by the 1D kernel over the simulation time step and the sources are re-distributed to the 3D gas phase based on the local number density of the kernel particles. The kernel moves and evolves while the energy is supplied by the ignition coil. At the end of the energized stage, the kernel radius is compared against the critical transition radius given by $S_T^* = 0$ [12,21] and if the found to be sustainable, G-scalar front is initiated from the current position of kernel's particles. Otherwise, the kernel is quenched, and a misfire is reported. Furthermore, when the kernel motion results in the arc length exceeding the critical value, set at 0.01m [22], the kernel is allowed to re-strike, whereby the new kernel is formed, and the detached kernel is evaluated against the critical radius and is either extinguished or allowed to develop into a G-scalar front.

After a successful ignition, the G-equation model is applied with the flame speed closure provided by a fully developed form of the turbulent flame speed used in the 1D kernel model:

$$\frac{S_T}{S_L} = 1 + A\left(\frac{u'}{S_L}\right)^{\frac{5}{6}} \quad (13)$$

with the single tuning coefficient A. G-scalar re-initialization mechanism was found to be essential for the accurate resolution of flame front propagation through the pre-chamber. Geometric re-initialization approach was implemented following [23]. The G-equation quenching model has been incorporated and tested [24]. A preliminary investigation reported in [24] did not result in significant quenching effects under similar conditions to these used in the present paper, therefore quenching model was disabled in simulations in order to reduce the simulation time.

Default first order in time, second order in space pressure-correction solver is used to resolve the flow field with a realizable k-e turbulence model using turbulent viscosity limiting after [25] with standard wall functions.

The RCEM-mounted pre-chamber simulations are performed with the same using Cartesian meshes. The computational mesh size was chosen based on a grid sensitivity study and comparison with LES simulations for the mixture formation analysis in pre-chamber [26]. Grids with 0.300, 0.240 and 0.180mm basic cell size in the pre-chamber have been evaluated with the same ratio of refinement from pre-chamber to the cylinder resulting in 835K, 1.6m and 3.14m total numbers of cells respectively. The average values do not exhibit significant grid dependency, for example average λ in pre-chamber at spark time varied by less than 5%. However fine grid was closer to the LES results [26] and was therefore used. The final grid had uniform spacing of Δx=0.18mm with two layers of near-wall refinement in the pre-chamber with a gradual expansion to 0.94mm in the main cylinder. No special clustering was employed in the flame jet region. The grid in the pre-chamber symmetry plane is illustrated in Figure 5 for one of the pre-chamber designs. Note that the y+ values vary substantially during the simulation because of the changing nature of the flow, with maximum y+ ~30 for most of the simulation duration. The y+ reaches maximum values when the fast flame jet propagates through the nozzles. For example, for a representative PC-A/ID003 case, y+ reaches the maximum of 150 at 711deg.

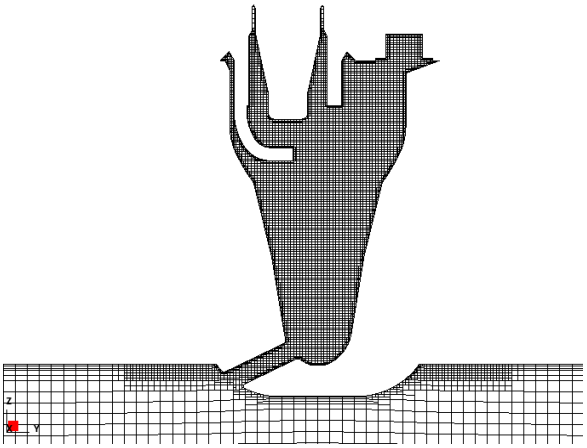

Figure 5. Grid schematic in the pre-chamber symmetry plane.

In simulations set-up, the injected mass and timings are determined from the experimental data. The injection profile was not measured, and a flat profile was assumed with 0.5ms linear ramp at the start and end of injection. Initial quiescent conditions for the simulations were specified based on the experimental data at -133.2deg. These exhibited very weak variability within RCEM runs. For a representative PC-A/ID001 case, the initial pressure in simulations was set to 1.36bar and the initial temperature to 383K. Constant temperature boundary conditions with all walls at 383K, based on the temperature-controlled environment in the RCEM experiment.

To facilitate comparative analysis a number of sensors were introduced in the model. Data is acquired from two volume sensors – the effective pre-chamber volume sensor comprising pre-chamber above the nozzles, and a 3mm spherical volume sensor around the centre of the spark plug gap to compare the local properties of the fuel/air mixture. In order to evaluate the jet exit time, seven surface sensors are introduced in the CFD simulation capping the exit points of the nozzles, with flow rates and flow rate averaged quantities acquired at these. The jet exit time threshold is defined by threshold value of burnt gas mass fraction in the mass flow rate through the sensors. Since this property cannot be directly compared with the experiment, where level of OH is used, the results are reported for a range of thresholds – 0.02, 0.04 and 0.045, and that the conclusions did not exhibit high sensitivity to the choice of the threshold.

Results

Spark Model Validation

The kernel model parameters selected based on the study reported in [12]. However, the new approach to the flame speed modelling necessitates validation of the complete model. Simulations of the spark ignition experiments reported in [17] for air/methane mixture at pressure 1-4bar and different λ=1.0-1.4 have been conducted with the same solver settings as for the pre-chamber simulations. Large grid size was used to ensure that the final radius in the 1D model does not exceed the dimension of the computational cell in effect enabling a purely 1D solution in the 3D CFD solver. The experiment of [17] corresponds to a quiescent vessel filled with homogenous mixture at constant pressure, with data acquired from time-resolved laser interferometry.

Figure 6 illustrates comparison of the kernel radius with the experimental data demonstrating good agreement across the range of simulated cases.

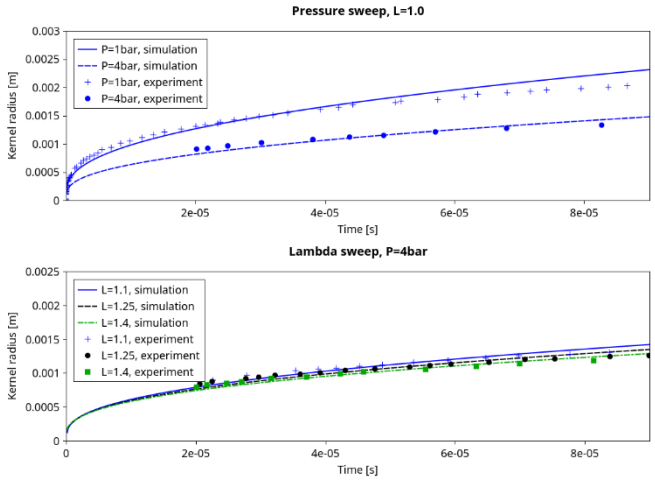

Figure 6. Spark ignition model validation for CH4-air mixtures (experimental data from [17]).

Pre-chamber Flow Topology and Mixture Formation

The differences in the flow structure between the pre-chamber designs and their effect on the mixture formation and combustion process is most visible when considering flow quantities just before the spark time for a representative injection case – ID002. The exact spark time exhibits variations between the pre-chambers, so the point selected to illustrate the differences corresponds to the earliest spark time for this case across the pre-chambers - 708.8deg. Figure 7 shows the distribution of the turbulent kinetic energy and λ at this point. The inclined nozzles of pre-chamber PC-A generate a spiral vortex attached to the pre-chamber surface with the high shear at the vortex boundary resulting in high levels of TKE. The vortex transports lean mixture from the main chamber into pre-chamber. This motion is offset by the downward vortex in the middle of the pre-chamber which transports fuel-rich mixture from the top of the pre-chamber. The straight nozzles of pre-chamber PC-C1, combined with the blockage provided by the spark body, force the nozzle-jets to join and attach to the wall close to the spark. This in turn creates a recirculation bubble with the downward flow along the wall of the pre-chamber opposite to the spark body. The bigger volume available at the bottom of pre-chamber PC-D2 causes detachment of the nozzle jets form the wall, which promotes mixing. Note that in all three cases there is a pocket of fuel-rich mixture next to the gas supply valve, however it is smallest in the PC-D2 design.

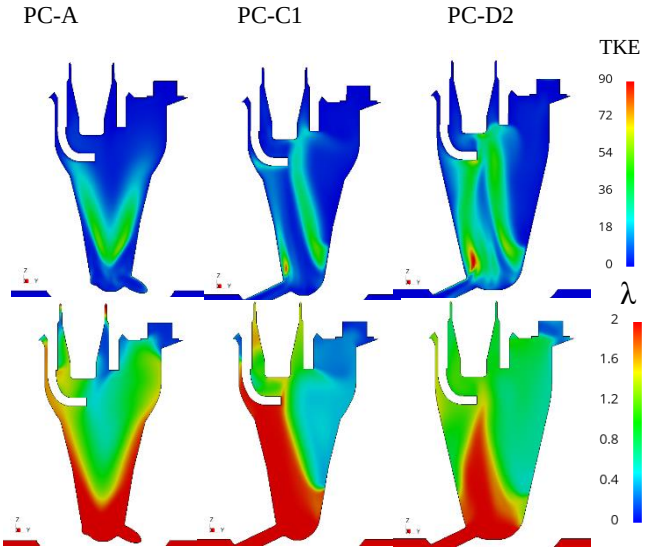

Figure 7. Flow topology at spark time: turbulent kinetic energy (top row) and the inverse equivalence ratio (bottom row)

The flow structure maps directly into the properties of the pre-chamber mixture. Considering the average values of λ and its variance in the pre-chamber volume sensor and the spark volume sensor illustrated in Figure 8, the same injected mass results in slightly lower average pre-chamber average λ for design PC-D2, due to its larger volume. However, the resulting mixture is more homogenous, as indicated by the lower variance of λ. Furthermore, the averages within the spark sphere show that the actual values in the vicinity of the spark obtained with this design are closer to stoichiometry and exhibit lower variation, which is beneficial for ignition.

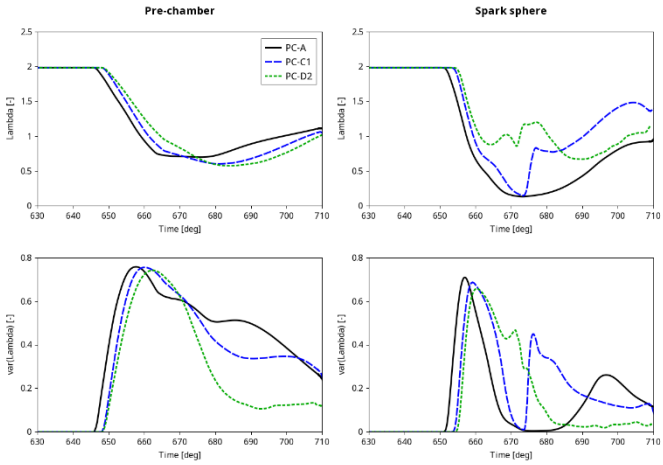

Figure 8. Inverse equivalence ratio and its variance in the pre-chamber and spark sphere sensors

Finally, PC-D2 delivers substantially increased turbulence levels near the spark plug (see Figure 9). The latter can be either beneficial or detrimental. Increased turbulence levels can deliver more rapid combustion, on the other hand excessive turbulence levels can pose danger to the sustainability of the initial flame kernel. The effect was found to be mostly beneficial, as the kernel quenching model as

formulated in the previous section did not show any occurrences of misfire in the conducted simulations.

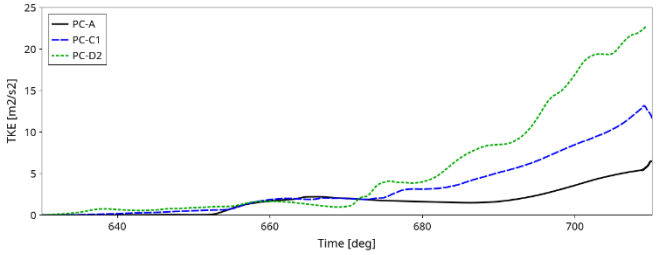

Figure 9. Turbulent kinetic energy in the spark sphere sensor

Combustion Process

The value of the tunable parameter A is in general case-dependent, for example a value of 2.8 was recommended in [27] for a GDI gasoline engine and 3.0-3.4 was explored in [28] for a large natural gas engine in lean conditions. In the present study, flame speed tuning was performed on a single case for the baseline pre-chamber PC-C1 and a medium injection condition ID002, resulting in A=2.75. This value was then used for all simulations. It was found to produce acceptable results across the range of simulated cases except for case ID001 corresponding to the smallest injected mass where the value of A=1.5 was required to recover the pressure peak matching the test data. However, it should be noted that the normalized standard deviation of the jet exit timing in the experimental data between repetitions is between 26 and 48% for the ID001 injection.

In all cases simulated, the flame kernel was generated, and no misfire occurred. The spark plug body effectively shields the spark plug gap so that local velocities are low. At the same time, scavenging ensures that the mixture is close to stoichiometry and the growth of the initial kernel is rapid. The length of path of the kernel from its initial position before the transition to the fully developed flame stage did not exceed the length of the spark plug gap in all simulated cases.

The comparison of pre-chambers in terms of turbulence levels persists during the ignition and firing stages of the combustion process. Figure 10 shows the average turbulent kinetic energy in pre-chamber and spark vicinity for the representative case ID003. Pre-chamber D2 shows higher levels of turbulence throughout the flame front development in the pre-chamber.

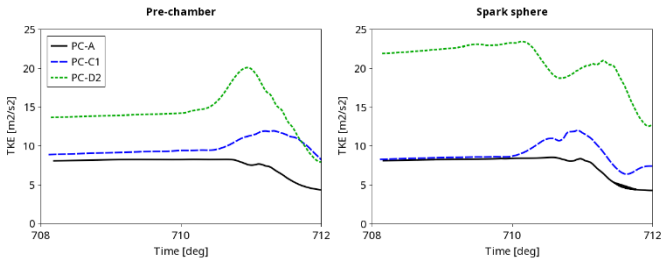

Figure 10. Comparison of pre-chamber and spark sphere turbulent kinetic energy during ignition and pre-chamber firing stages for case ID002.

Higher levels of turbulence during the combustion process lead to a more rapid flame development in the pre-chamber. Figure 11 shows the contours of temperature at 712deg, when the flame jet reaches the piston in the main cylinder in the fast cases. Pre-chamber D2 shows faster flame propagation in the cylinder as well as a less diffuse flame front, pointing to a higher momentum of the flame jet.

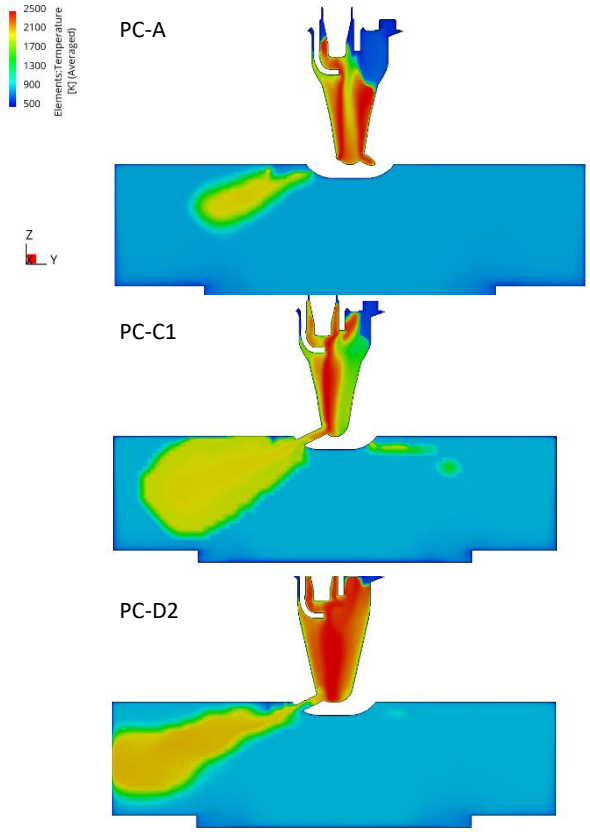

Figure 11. Turbulent kinetic energy in the spark sphere sensor

The flow topology in the pre-chambers and different levels of turbulence affect not only the speed of combustion but also the momentum of the flame torch. Figure 12 illustrates the mass flow rate through nozzle sensor 1 in a representative case ID003. To enable comparison time axis is shifted to 0 at spark time. Pre-chamber PC-D2 delivers more power to the flame jets even though the spark time is later by 1.2deg by comparison with PC-A, i.e. the flame propagates against higher counter-pressure. Nozzle surface sensors also indicate that there is an oscillating flow pattern with flow reversal observed as pre-chamber fires against the compression driven by the piston. Note that the rapid drop of the mass flow rate corresponds to the point where the flame reaches the main cylinder leading to a rapid increase of pressure downstream of the nozzles in the main chamber.

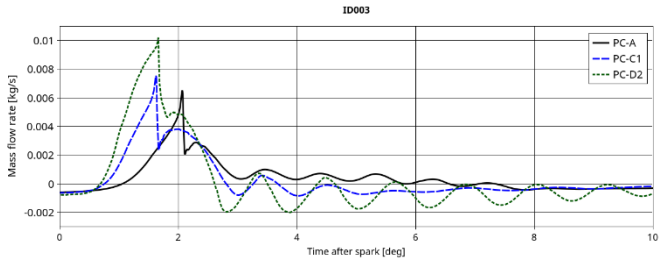

Figure 12. Mass flow rate through pre-chamber nozzles (simulation)

The resulting pressure trace and heat release rate comparison with the experiment is illustrated in Figure 13 for a representative case ID003. The homogeneity and turbulence levels arguments of the previous section translate readily to the combustion process. More homogenous pre-chamber PC-D2 with larger turbulence levels delivered the largest pressure increase and most rapid combustion for the same injected fuel mass. The smaller volume pre-chamber PC-C1 delivered slower combustion. Pre-chamber PC-A demonstrated worst performance. The same trend was observed for all simulated injection cases and comparative ranking of pre-chambers with respect to the pressure peak and speed of combustion for the same injected fuel mass remained the same as observed in the test data.

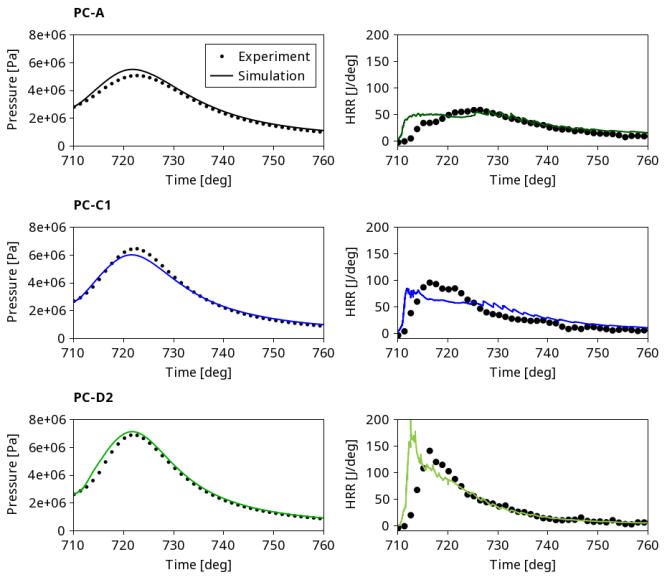

Figure 13. Main chamber pressure and heat release rate comparisons for case ID003.

The differences in the instantaneous heat release rate map to differences in cumulative heat release shown in Figure 14.

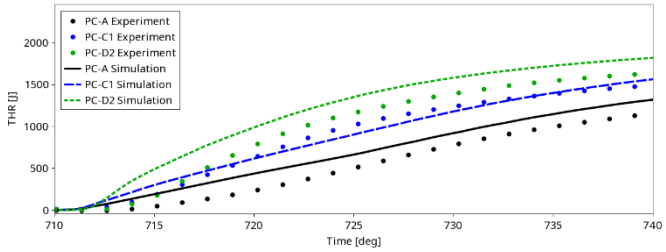

Figure 14. Comparison of THR for case ID003

Figure 15 illustrates the flow asymmetry through the comparison of mass flow rates for all nozzles for case ID003 in two best performing pre-chambers. Flow topology in pre-chamber PC-C1 results in a higher asymmetry of the mass flow rate after the initial jet reaches the nozzle. This slight asymmetry was also observed in the simulations of this pre-chamber mounted on the target engine [7]. Note that for the set of pre-chambers and injection cases presented in this study, no direct comparison of OH* chemiluminescence has been made and hence it is difficult to ascertain this behaviour. However in a similar study performed for a different set of conditions for PC-A [30], the degree of asymmetry has been observed to be similar between the experiment and the simulation.

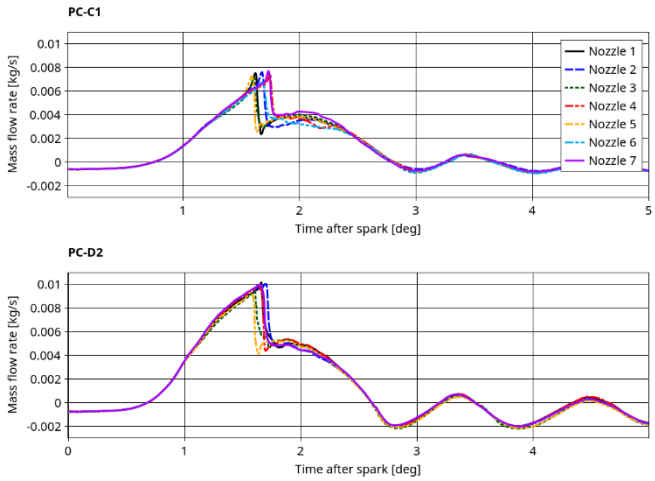

Figure 15. Flow asymmetry through pre-chamber nozzles, case ID003, (simulation)

Figure 16 shows the comparison of jet exit times with the experimental data with variable threshold for flame exit point. The jet exit times are predicted well, with little sensitivity to the threshold value, apart from the lean scavenging case ID001. This correlates with the experimental observations of high standard deviation observed in RCEM experiment repetitions for this case. The slower combustion in case ID001 results in a more diffuse flame front by the time the flame reaches the nozzles, which in turn leads to higher variation in the jet exit times based on different thresholds. The overall tendency in the simulation is to result in faster jet exit times than these observed experimentally, this is further illustrated by the pressure traces from the pre-chamber presented in Figure 17. Note that the flow reversal observed in the simulations for the pre-chamber PC-D2 is clearly visible in the pre-chamber pressure traces in the simulations but is not pronounced in the experiment.

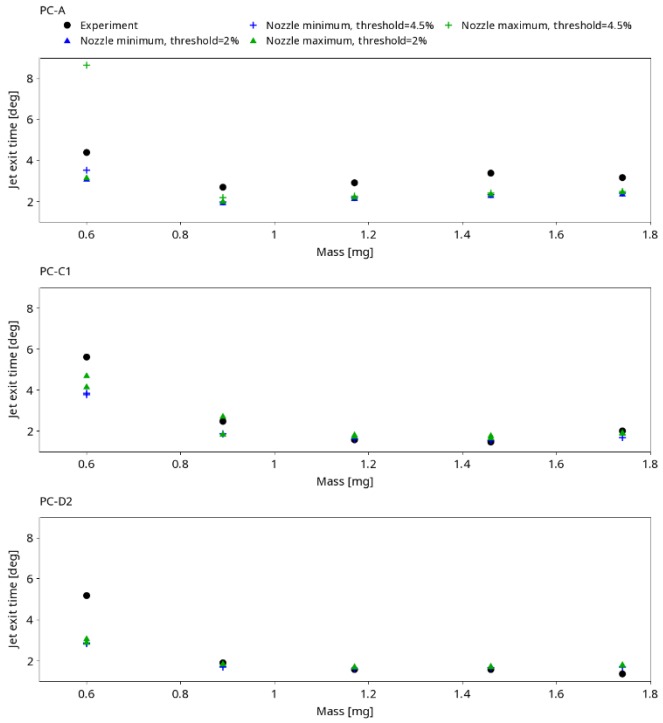

Figure 16. Comparison of jet exit times between the simulation and experiment with different threshold criteria

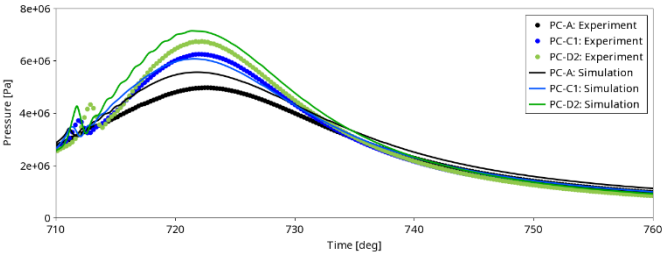

Figure 17. Comparison of pressure traces in pre-chambers between the simulation and experiment

Conclusions

Three designs of pre-chambers developed within Horizon 2020 GASON project have been compared through a combined experimental and numerical investigation, in order to evaluate the effects of the tangential nozzle angle and volume variation. Conclusions obtained through both methods are identical and favor the design with straight nozzles and larger volume, which delivers better mixing, more rapid combustion and higher energy flame jets for the same injected fuel mass. The insights obtained from the CFD study provide a clear explanation of the observed differences based on the flow topology.

The proposed CFD model incorporating spark ignition model and combustion model demonstrates good accuracy in basic validation studies and correctly describes relative performance of the studied pre-chambers across a wide range of pre-chamber injection parameters with a single parameter tuning for the empirical turbulent flame speed correlation. The exception to the above is the lean scavenging case, however in this case a very high standard deviation in the experimental data is observed as well.

It is worth pointing out that while the conclusions are clear for the current study, there is an inherent challenge in transferring insights concerning engine performance derived from the comparison of the pre-chambers mounted on an RCEM to the actual target engine. Firstly, because of much higher levels of combustion chamber turbulence and complex main charge flow in the latter, secondly because of the interaction between the pre-chamber and piston shape being an essential factor. For example, simulations for the target engine with pre-chamber PC-C1 and a hemi-spherical piston bowl conducted in [7] show a more substantial flow asymmetry by comparison with the observations of the present study. The evaluation of the proposed increased volume design and further analysis of these pre-chambers in single and multi-cylinder engine installations are ongoing.

References

1. Ricardo, H.R., “Recent Work on the Internal Combustion Engine”, SAE Transactions, Vol 17, May 1922.

2. Toulson, E., Schock, H. J. and Attard, W. P., “A Review of Pre-Chamber Initiated Jet Ignition Combustion Systems”, SAE Technical Paper 2010-01-2263, 2010.

3. Gussak, L., Karpov, V., and Tikhonov, Y., “The Application of Lag-Process in Prechamber Engines,” SAE Technical Paper 790692, 1979, doi:10.4271/790692.

4. Attard, W., Kohn, J., Parsons, P., “Ignition Energy Development for a Spark Initiated Combustion System Capable of High Load, High Efficiency and Near Zero NOx Emissions,” SAE Journal Paper JSAE 20109088, 2010.

5. Horizon 2020 GASON Project, http://gason.eu/

6. Soltic, P., Hilfiker, T., Hänggi, S., Hutter, R., and Weißner, M., "Ignition and combustion concepts for lean operated passenger car natural gas engines", Proc. 12th Conference on Gaseous-Fuel Powered Vehicles, Stuttgart, 2017.

7. Lucas, G., Tallu, G. and Weißner, M., "CFD-based Development of an Ignition Chamber for a lean and highly efficient CNG Combustion", Proc. THIESEL 2018 Conference on Thermo- and Fluid Dynamic Processes in Direct Injection Engines, 2018.

8. Vlaskos, I., Majer, J., Letrich M. and Kolda, J., "Pre-Chamber Design Criteria for High Efficiency Gas Engines", Proc. 28th CIMAC World Congress, Helsinki, 2016.

9. Schlatter, B. Schneider, Y.-M. Wright, K. Boulouchos, Experimental study of ignition and combustion characteristics of a diesel pilot spray in a lean premixed methane/air charge using a rapid compression expansion machine, SAE Technical Papers 2012-01-0825. https://doi.org/10.4271/2012-01-0825

10. Testem, Technical Manual TeRCM-K48: Rapid Compression Machine for in-cylinder spray development and combustion processes analysis. Testem - Gesellschaft für Mess- und Datentechnik GmbH, Hoflach No. 5, D-82239 Hoflach/Alling, 2004

11. M. Weissner, F. Beger, C. Klüting, G. Lucas, T. Hilfiker, "GasOn: a lean CNG Combstion for highest engine efficiencies above 43% utilizing an ignition chamber", SAE Torino CO2 Reduction for Transportation Systems Conference, Turin, July 2018

12. Tallu, G., Beck, L. M., Prouvier, M., Winkler, A. and Shapiro, E., "3D CFD Modelling and Simulation of Spark Ignition Inclusive of Turbulence Effects and Detailed Chemical Kinetics", Proc. 3rd International Conference on Ignition Systems for Gasoline Engines, November 3–4, 2016, Berlin

13. Chen C., Bardsley, M.E.A. and Johns, R.J.R., "Two-Zone Flamelet Combustion Model", SAE Technical Paper 2000-01-2810, 2000.

14. Tan, Z. and Reitz, R.. "Modeling ignition and combustion in spark-ignition engines using a level set method", SAE Technical Paper 2003-01-0722, 2003.

15. Herweg R. and Maly, R. R. "A fundamental model for flame kernel formation in S.I. engines". In SAE International, 922243, 1992.

16. Sher, E., Ben-YaIsh, J. and Kravchik, T., "On the birth of spark channels", Combustion and Flame, 89:168-194, 1992.

17. Maly, R. and Vogel, M., "Initiation and propagation of flame front in lean ch4-air mixture by the three modes of the ignition spark", Proceedings of the 17th Symposium (international) on Combustion, The Combustion Institute, 17, pp. 821-831, 1978.

18. Shapiro, E., Tiney, N. "Advanced Ignition Modelling for Pre-chamber Combustion in Lean Burn Gas Engines", Proc. 4th International Conference on Ignition Systems for Gasoline Engines, Berlin, December, 2018

19. Hinze, J. O., "Turbulence", McGraw–Hill, New York, Second edition, 1975.

20. Metghalchi, H. and Keck, J.C.: Burning velocities of mixtures of air with methanol, iso-octane, and indolene at high pressure and temperature. Combustion and Flame 44 (1982) 1081–1093.

21. Ewald, J. and Peters, N., "On unsteady premixed turbulent burning velocity prediction in internal combustion engines.", Proceedings of the Combustion Institute, 31:3051–3058, 2007.

22. Dahms, R., Fansler, T.D., Drake, M.C., Kuo, T.-W., Lippert, A.M. and Peters N., "Modelling ignition phenomena in spray-guided spark-ignited engines", Proc. of Comb. Institute, 32:2743–2750, 2009.

23. Reinecke, M., Hillebrandt, W., Niemeyer, J. C., Klein, R. and A. Gröbl. "A new model for deflagration fronts in reactive fluids", Astron. Astrophys., 347:724–733, 1999.

24. Hernández, I., Shapiro, E., Tiney, N., Kotzagianni, M., Kyrtatos, P. and Boulouchos, K., "Flame-wall interaction modelling for pre-chamber combustion in lean burn gas engines", Proceedings of 34th International CAE Conference and Exhibition, 2018, Vicenza, Italy

25. Przulj, V., Tiney, N., Shapiro, E., Penning, R. and Shala, M., "The time scale bounded k-e turbulence model and its assessment for automotive applications", Proc. 7th Int. Symp. Turbulence, Heat and Mass Transfer, Palermo, Italy, 2012

26. Bolla, M., Shapiro, E., Tiney, N., Kyrtatos, P., Kotzagianni, M., Boulouchos, K., "Numerical study of turbulence and fuel-air mixing within a scavenged pre-chamber using RANS and LES", Submitted to SAE World Congress and Exhibition, Manuscript no: 19PFL-0664

27. Schmitt M., Hu, R., Wright, Y. M., Soltic P. and Boulouchos K. "Multiple Cycle LES Simulations of a Direct Injection Methane Engine," Flow, Turbulence and Combustion (95):645–668, 2015

28. Xu, G., Hanauer, C., Wright, Y., and Boulouchos, K., "CFD-Simulation of Ignition and Combustion in Lean Burn Gas Engines", SAE Technical Paper 2016-01-0800, 2016, doi:10.4271/2016-01-0800

29. Lipatnikov A.N. and Chomiak J., "Turbulent flame speed and thickness: phenomenology, evaluation and application in multi-dimensional simulations", Prog. Energy Comb. Science, 28, 2002 (1-74).

30. Bolla, M., Shapiro, E., Tiney, N., Kyrtatos, P., Kotzagianni, M., Boulouchos, K., "Numerical simulation of pre-chamber combustion in an optically accessible RCEM ", Submitted to SAE World Congress and Exhibition, Manuscript no: 19PFL-0668

Contact Information

Dr Evgeniy Shapiro
Ricardo Software, Shoreham Technical Centre, Shoreham by Sea, BN43 5FG, UK
Phone: +44(0)1273794802
Fax: +44(0) 1273794553
evgeniy.shapiro@ricardo.com

Acknowledgments

This work has been supported by the European Union's Horizon 2020 GASON research and innovation programme under grant agreement No 652816.